Effects of Thermal Conduction in Microchannel Gas Coolers for Carbon Dioxide

Pietro Asinari[a], Luca Cecchinato[b], Ezio Fornasieri[*b]

[a]*Dipartimento di Energetica, Politecnico di Torino, Corso Duca degli Abruzzi 24, I-10129 Torino, Italy*

[b]*Dipartimento di Fisica Tecnica, Università degli Studi di Padova, via Venezia 1, I-35131 Padova, Italy*

[*] Corresponding Author. Tel.: +39 049 827 6878; fax: +39 049 827 6896; e-mail: ezio.fornasieri@unipd.it - Member of IIR Commission B2

Abstract

A numerical code was developed for an accurate fully three-dimensional simulation of crossflow compact heat exchangers with finned, internally microchannelled flat tubes, which are often used as gas coolers in transcritical refrigerating machines CO_2 operated. The equations describing the system were discretised by means of a finite-volume and finite-element hybrid technique for strictly adhering to the real heat transfer process regarding the finned surfaces. The numerical code uses recent correlations by different authors for predicting the heat transfer coefficients both refrigerant side and air side. The results of simulations are verified against experimental data reported in the open literature.

The aim of this work is to investigate the effects of thermal conduction inside metal on the overall performance of the considered gas coolers; high-resolution meshes for the discretisation of separating wall and fins makes it possible to avoid much of the approximations typical of the traditional approaches. In particular the efficiency of finned surfaces, the real distribution of thermal fluxes between the two fin roots and the effects of thermal conduction along the walls of microchannel flat tubes are extensively discussed.

The numerical simulations confirm that the traditional approach for describing fins, which assumes them as adiabatic at the middle section in order to decouple the equations accounting for the effect of different temperatures at the fin roots, can be considered acceptable in a wide range of applications. In a similar way, the conduction on fins along the direction of the air velocity and the longitudinal conduction on tubes produce a negligible effect on the performance of the considered class of heat exchangers.

Keywords: Refrigerant; Carbon Dioxide; Transcritical cycle; Gas Cooling; Design; Heat Exchangers; Modeling.

1. Introduction

Finned heat exchangers made of flat extruded aluminium tubes with internal microchannels are a topical subject, both from the technological and the scientific point of view. With respect to the traditional finned coil heat exchangers, they appear to have a better energy efficiency, in terms of larger heat transfer capability being the same the mechanical power spent for circulation of the working fluids. This is true both for the inside and outside sides of the heat exhanger.

Furthermore, microchannel tubes, because of their high mechanical resistance to the internal pressure, are a suitable solution for gas cooling in CO_2 transcritical cycles. The optimisation of this type of heat exchanger is therefore one of the main research goal for the development of refrigerating systems operated by this natural fluid.

The CO_2 transcritical cycle differs much from a traditional vapour compression cycle: a fundamental difference is that the upper pressure is not any longer related to heat transfer condtions of a condenser, but is a parameter subjected to optimisation since its value, as well as the gas temperature at the throttling valve inlet, has a great impact on the thermodinamic efficiency of the cycle. High thermal efficiency of gas cooler is an essential condition to obtain high COP values, since a low value of the CO_2 temperature at its outlet increases the cooling capacity, so allowing a reduction of the upper pressure and thus of the mechanical compression power. In fact, the optimal upper pressure value can be regarded, at a rough estimate, as inversely proportional to the gas cooler thermal efficiency.

The gas cooler analysis, aimed at optimising its design, faces the problem related to the wide variations of the thermodinamical and thermophysical properties near the critical point: using a high-resolution mesh is the mandatory solution.

The aim of this work is to analyse the possible drawbacks of the common assumptions used to simplify the solution of the equations related to conduction inside metal. To this end, a code was developed, which takes into account the real distribution of heat flux due to transverse and longitudinal conduction along both tubes and fins. In the following sections, the physical model and the implemented discretisation will be illustrated and some results of a simulation will be discussed.

2. The numerical code

Since crossflow compact heat exchangers with microchannelled flat tubes provide high thermal efficiency, they are widely utilised as gas coolers in transcritical refrigeration machines with CO_2 as the operating fluid [1]. These components conceptually belong to the general class of crossflow heat exchangers and they look as the one shown in Fig. 1(a).

For convenience, the calculation domain is subdivided into a wall domain Ω_w, which identifies all metal parts, and a fluid domain Ω_f, which identifies all volumes containing fluids. The fluid domain is constituted by many fluid paths, each one characterised by a proper dimensionless coordinate $0 \le x_i = X_i / l_i \le 1$. The physical model, defined over the whole computation domain, is expressed by the following equations.

$$P \in \Omega_f \qquad G_i\left[h_i(x_i) - h_i(0)\right] = \int_0^{x_i} \alpha_i\left[T_w(y_i) - T_i(y_i)\right] A_i \, dy_i \tag{1}$$

$$p_i(0) - p_i(x_i) = \frac{G_i^2}{2\rho_i}\left(f_i \frac{l_i x_i}{d_i} + \xi_i \right) \tag{2}$$

$$P \in \Omega_w \qquad \nabla(k_w \nabla T_w) = 0 \tag{3}$$

The overall thermal balance for the heat exchanger can be expressed as:

$$\int_{\partial\Omega_w} \nabla(k_w \nabla T_w) dV = \sum_{i=i}^{N_c} G_i \left[h_i(1) - h_i(0)\right] - \sum_{j=i}^{N_h} G_j \left[h_j(0) - h_j(1)\right] = P_c - P_h = 0 \qquad (4)$$

For solving the system of equations (1), (2), (3) and (4), a proper set of boundary conditions is needed. Usually for equations (1) and (2), Dirichlet-type conditions at the fluid inlet for enthalpy $h_i(0)$ and pressure $p_i(0)$ are imposed. On the other hand for equation (3), a Neumann-type condition is imposed on the portion of the wall surface A which is in contact with the external environment. Since the heat exchangers are usually well insulated, a zero value is set for this heat flux ($\partial T_w / \partial n = 0$ for $P \in \partial\Omega_w \cap A$). The phenomenological coefficients which characterise heat transfer (α_i) and pressure drops (f_i and ξ_i) are evaluated according to common correlations reported in the open literature (see Tab. 1).

The described physical model is characterised by strong coupling among equations, mainly due to equation (3), which depends on the temperature profile inside the metallic walls. According to the purpose of this work, the effects of thermal conduction is investigated without any simplifying hypothesis regarding the coupling of equations. Recently, a general numerical approach for heat exchangers, dubbed Semi-Explicit Method for Wall Temperature Linked Equations SEWTLE, has been proposed [7]. This method decouples the calculation of the wall temperature field from that of fluid temperature and computes the final solution by means of an iterative procedure which is brought to convergence by verifying the enthalpy balance between hot-side and cold-side. In particular, a guess profile for temperature inside metallic wall is assumed as the starting point; on this basis, the convective thermal fluxes is calculated by means of equations (1) and (2). Then a new distribution of wall temperature, which will be closer to final solution, is determined by equation (3). This iterative procedure continues until the condition (4) is satisfied within the desired tolerance.

In order to create a numerical code for simulating the physical model, a discretisation technique must be considered. According to the Finite Volume Method (FVM) [8], the flat tubes are discretised into elementary control volumes, characterized by centroids located at intersections between the fins and the separating walls that identify microchannels, as shown in Fig. 1(b). The same techniques is applied to the fluid domain: numerical convenience suggests to introduce a transversal dislocation between fluid and tube centroids [9], as shown in Fig. 1(c). The application of the FVM to fins discretisation would increase beyond reasonableness the number of nodal values in order to obtain a sound accuracy: for this reason the Finite Element Method (FEM) was employed. Unfortunately, the technique of classical surrounded elements does not ensure the thermal continuity needed by the SEWTLE approach. Then an intrinsically conservative element was introduced for the FEM definition of fins, as shown in Fig. 2(a), which is compatible with the SEWTLE technique [9], since the shape function (5) coincides with the exact solution of the equations of the convective heat transfer in fins, under some simplifying hypotheses [10].

$$\theta(y,z) = C_1 \exp(\omega y) + C_2 \exp(-\omega y) + C_3 \exp(\omega z) + C_4 \exp(-\omega z) \qquad (5)$$

where $\omega = \sqrt{\sum \alpha_i / (k_w s)}$ is the inverse of a characteristic length and $\theta(y,z) = T_w(y,z) - \sum \alpha_i T_i / \sum \alpha_i$ represents the effective temperature difference. The couple of temperature at fin roots and the conductive heat fluxes at remaining borders constitute a proper set of boundary conditions to calculate the constants C_i. In particular this set makes the element intrinsically conservative and produces an accurate description of temperature profile, as shown in Fig. 2(b).

The described discretisation scheme is an hybrid one, which adopts both FVM and FEM to avoid simplifying hypotheses, providing therefore high accuracy, without demanding too much calculation resources.

3. Comparison with experimental data

In order to verify the reliability of the numerical code, a comparison between simulation results and experimental data was carried out. The experimental data were found in [11] and cover a wide range of operating conditions of the gas-cooler for automotive applications depicted in Fig. 3. The simulation speed and the results accuracy depend on the number of nodes of the grid in the section of microchannelled tube; the best definition is the one that considers the number of virtual microchannels equal to the real case, but a smaller number can be chosen for simplifying the calculation.

In Fig. 4, the calculated values of the total heat transfer rate are reported against the experimental values; the simulation slightly overestimate the real thermal performance, but the accuracy is high, since most of the errors are smaller than 3%, being the maximum error around 6%. Even if from these results the simulation model appears reliable and accurate, it is worth noting that this high accuracy could be related to the high thermal efficiency of the gas cooler, that makes the thermal power not very sensitive to the heat transfer characteristics. Furthermore, the total heat flow exchanged is strongly dependent on the correlations chosen to evaluate the heat transfer coefficients. On the other hand, applying the direct numerical analysis of convective heat transfer has been considered impractical, because it would have required a tremendous increase in the mesh size.

It is interesting to investigate the effect of the mesh resolution on the final results, since in transcritical CO_2 cycles the modelling of the cooling process at high pressure raises some problems related to transformation close to the critical point, where very large variations of the thermodynamical and thermophysical properties occur.

To this end, a dimensionless parameter, $D = \sqrt{\left[p_{in}/p_{cr} - 1\right]^2 + \left[h_{in}/h_{cr} - 1\right]^2}$, was proposed by the authors to quantify the proximity of the operating conditions to the critical point.

Although the error distribution is quite scattered, as shown in Fig. 4(b), the trend curve with reasonable accuracy can be described by eq. (6) which clearly demonstrates that errors increase when the system is operating near the critical point:

$$E = E_0 \exp(-D/D_0) \tag{6}$$

To analyse the sensitivity of the simulation errors to the mesh resolution, the calculation for Test n° 9 [11], which is a critical case for the operating conditions, was repeated, increasing the number of nodes from the most simplified case. Increasing the number of nodes brings about a better accuracy in representing the thermal fields in the system and from a physical point of view is equivalent to increase the number of virtual microchannels inside the flat tube. When the number of virtual microchannels is equal to the real number of microchannels in the gas cooler, the maximum possible accuracy is reached. The results of this comparison are shown in Tab. 2; increasing the number of virtual channels from 1 to 3 greatly improves the accuracy in evaluating heat flow, but a further increase in the mesh resolution does not produce a significant benefit. In the same Tab. 2 the total heat flow was subdivided into three contributions, referring to the three sections of the heat exchanger, corresponding to the three gas passages; the deviations of the calculated values for different numbers of virtual channels with respect to the most simplified case (one virtual channel) can give an account of the effect of the mesh size on the heat transfer prediction for heat exchanger of different effectiveness, or subjected to different heat flow: as expected, when comparing the

deviations for Section I and for the whole heat exchanger, high heat flux calls for high resolution, because the consequent high temperature gradients require more detail in describing the process.

As far as the pressure drop of the refrigerant is concerned, in [12] it is asserted that the most of the traditional correlations underestimate the experimental data: this has been confirmed by the results of the simulations, which show an average mean error of –70% in predicting pressure drop. To investigate the effect of this variable on heat flow, simulations have been carried out having increased, according to different multiplying factors, the values of pressure drop calculated from the correlations reported in Tab. 1. The results in Tab. 3 point out small improvement in the prediction of heat flow and highlight small sensitivity of the heat transfer performance to pressure drops.

4. The thermal conduction in fins

The numerical code described in the previous sections can investigate some phenomena usually neglected in evaluating the fins efficiency. In modelling compact heat exchangers as the one shown in Fig. 1, an usual approximation is employed, consisting in the half-fin-length idealisation. According to this idealisation, the section of the fin at the middle distance from the tubes is assumed as adiabatic; this is strictly true only when the fin bases are both at the same temperature. In a real case, these temperatures in general are different and, as a consequence, the adiabatic line is shifted from the middle position and unequal lengths of fin transport heat to the tubes at its roots. In extreme cases, the adiabatic line is not present on the fin and the two tubes are subjected to opposite heat flows (entering one tube and exiting from the other).

The transverse heat flows for unit length q_A and q_B at fin roots A and B can respectively be expressed by the following correlations [13]:

$$q_A(y) = \frac{s\omega\sqrt{2}}{\sinh(\omega z_0)} k_w \left[\theta_A \cosh(\omega z_0) - \theta_B\right] = q_A^*(y) + \frac{s\omega\sqrt{2}}{\sinh(\omega z_0)} k_w \left(\theta_A - \theta_B\right) \tag{7}$$

$$q_B(y) = \frac{s\omega\sqrt{2}}{\sinh(\omega z_0)} k_w \left[\theta_B \cosh(\omega z_0) - \theta_A\right] = q_B^*(y) - \frac{s\omega\sqrt{2}}{\sinh(\omega z_0)} k_w \left(\theta_A - \theta_B\right) \tag{8}$$

where z_0 is the fin height, q_A^* and q_B^* the heat flows per unit length predicted by the half-fin-length idealisation. To discuss the adequacy of this idealisation, a splitting factor is introduced:

$$r = \int_0^{y_0} q_A(y)dy \Big/ \int_0^{y_0} \left[q_A(y) + q_B(y)\right]dy \tag{9}$$

where the heat flows due to thermal conduction is considered positive if entering the fin. The half-fin-length idealisation is exactly complying with reality when the temperature differences at both ends are equal $\theta_A = \theta_B$; in this case the splitting factor is $r = 1/2$. For most of the typical operating conditions of multi-stream plate fin heat exchangers, this condition is very close to be fulfilled and half-fin-length approximation produces acceptable errors. When θ_A greatly differs from θ_B, the splitting factor are far from 1/2 and therefore in these cases the half-fin-length idealisation is not any longer acceptable.

Another approximation widely employed in modelling heat transfer with extended surfaces suggests to neglect the thermal conduction directed along the direction of air flow. For louvered fins, the longitudinal conduction can be taken into account through a suitable value of an equivalent directional thermal conductivity.

To show the potential of the present numerical code and to verifying the accuracy of the simplifying hypotheses of common use, a simulation was performed for the compact heat exchanger shown in Fig. 3. In particular Test n° 32 [11] is considered: the mass flow rate of carbon dioxide is 26 g/s, the inlet pressure is 76 bar and the inlet temperature is 78.2 $°C$, while for air the mass flow rate is 454 g/s and the inlet temperature is 26.8 $°C$.

In Fig. 5 the contour lines of the splitting factor are reported for the face area of the heat exchanger; this variable is not defined in all point of the face area, but only for fins and consequently the curves are built by linking points located on the fins; moreover, in the definition of splitting factor (9), subscript A refers to the upper fin root, so that $r > 1/2$ means that the upper thermal flux is greater than lower one.

Only few fins are characterized by splitting factors far from ideal value $r = 1/2$; they are located between flat tubes which are close to different refrigerant passages, where the temperature difference between the refrigerant flowing inside adjacent tubes is large. In this situation the half-fin-length idealisation introduces a significant error in estimating the distribution of thermal fluxes and the related temperature field inside the metal. However since $q_A^* + q_B^* = q_A + q_B$, as follows from equations (8) and (9), it can be concluded that the half-fin-length idealisation correctly predicts the total heat transfer from/to a fin, but it is wrong in predicting the individual heat flows at the roots. This involves a modest effect on the prediction of the total heat transfer rate, as results from Tab. 4.

In Fig. 6 some relevant values of the thermal variables are shown for different section of a fin, subdivided into vertical strips linking two adjacent tubes. The values inside the circles show the convective heat flow exchanged with air on both fin sides. The values at the fin root show the heat flow entering (negative value) or exiting (positive values) from the tubes; the values inside parentheses refer to heat flow predicted by half-fin-length idealisation. The temperatures at the fin roots are printed outside the fin contour. The longitudinal heat flow transferred by conduction is indicated next the related arrows. For the considered fin, the splitting factor is equal to $r = 2.47$, which is very close to maximum value in Fig. 5, and entails a reversed conductive flux (i.e. from the fin to the tube) at the lower fin root. The sum of heat flow entering both the fin bases is equal to 440 mW, as predicted by half-fin-length idealisation, according to theory. The longitudinal conductive heat flow in the direction of the air flow shows its maximum at the central portion of the fin, while is very small at both fin ends; anyway the maximum value, which is equal to 12 mW, is nearly negligible if compared with the transverse conductive heat flow.

5. The thermal conduction in microchannelled tubes

It is common practice to consider the wall temperature of the tubes uniform on any cross section and to neglect the heat flowing longitudinally by conduction through the walls, even if longitudinal temperature gradients exists. Instead, the present simulation code takes into account these aspects of heat transfer and therefore can quantify the error associated to the mentioned simplifying assumptions.

In the following Figg. 7 and 8 some of the numerical results obtained with the simulation code are reported, referring to the operating conditions of Test n° 32 [11], already considered in Fig. 5.

A factor σ has been defined to take into account the non-uniformity of the temperature field in the cross section of microchannel tubes:

$$\sigma = \sqrt{\sum_{i=1}^{N} A_i \left(T_i - \sum_{i=1}^{N} A_i T_i \Big/ \sum_{i=1}^{N} A_i \right)^2 \Big/ \sum_{i=1}^{N} A_i} \qquad (10)$$

The contour lines of factor σ for the cross sections of microchannel tubes are plotted in Fig. 7. Notwithstanding the σ factor is a variable defined only for the tube section, for the sake of readability, the curves are built by linking all points with equal σ values (the same for the following Fig. 8).

According to heat flux resulting from simulation, compared with the one of an ideal case with isothermal cross section, it follows that the common assumptions can be considered fully acceptable. This holds also for most critical sections located at the inlet of refrigerant where there is the maximum temperature differences between the fluids and consequently the maximum heat flux.

In Fig. 8 the contours lines of the longitudinal heat flow by conduction along the tube walls (in the direction of the refrigerant flow) are plotted. The numerical results of Fig. 8 show that the longitudinal heat flow can be neglected in evaluating the heat transfer process in such a kind of heat exchanger, also for the tubes subject to the maximum temperature gradients. In fact, the order of magnitude of the overall heat flow for a single tube is about one hundred Watt.

6. Final remarks

At last, a sensitivity analysis has been carried out about the influence of the heat transfer coefficients and the thermal conductivity of the metal for both fins and tubes on the heat transfer capability of the heat exchanger; to this purpose simulations were performed, increasing these parameters by 20%, one at a time. The results of simulations reported in Tab. 5 show that the increase in the air side heat transfer coefficient has comparatively the largest effect because it acts on the side where the largest thermal resistance exists, but this effect is nevertheless rather small, because of the high thermal efficiency of the heat exchanger.

To complete the analysis of the effect of the thermal conduction inside the metal, with reference to the simplifications assumed in the traditional numerical codes, other simulations have been performed, setting to zero, one at a time, the thermal conductivity along different axes, excepting the one orthogonal to the fin bases. From the results, shown in Tab. 6, it can be inferred that the longitudinal conduction, both in fins and tubes, and the transverse conduction in tubes are not significant for thermal process; thence it results that the traditional calculation procedures, even if they do not take into account these effects, nevertheless do not suffer any significant loss of accuracy in relation to these simplifications.

Conclusions

A numerical simulation model for compact heat exchangers which takes into account the effect of thermal conduction along the fins and the walls of tubes was developed to analyse the effect of the simplifying assumption used in the classical approach.

The conclusions drawn from the analyses are:

a) The models using the half-fin length idealisation, although do not accurately represent the real distribution of heat flow between the fin roots, when the temperatures at the fin bases are different, nevertheless give a reasonably accurate prediction of the total heat flow exchanged.
b) The longitudinal conduction in fins, the transverse and the longitudinal conduction in tubes give negligible effects on the total heat flow and on the temperature field.

The innovative numerical code here presented certainly offers improved accuracy, with respect to the simplified simulation models, in predicting the thermal variables and the total heat flow: although in most cases the accuracy of the simplified models can be regarded as acceptable, when

thermal conduction assumes a key role in determining the heat flow (low metal thermal conductivity, low wall thickness, high convective heat transfer coefficients) there is a need for a more sophisticated modelisation, as the one described in the present paper.

Nomenclature

A	area [m^2]	s	fin thickness [m]
d	hydraulic diameter [m]	V	volume [m^3]
f	friction factor for distributed pressure drop [-]	T	temperature [K]
G	mass flow rate [kg/s]	α	convective heat transfer coefficient [$W/(m^2K)$]
h	specific enthalpy [J/kg]	ζ	friction factor for concentrated pressure drop [-]
k	thermal conductivity [W/(mK)]	ρ	density [kg/m^3]
P	heat flow [W]	σ	temperature field variance [K]
p	pressure [Pa]	ω	The inverse of a characteristic length [1/m]
q	Heat flow for unit length [W/m]	θ	Effective temperature difference [K]
r	splitting factor [-]		

Subscripts:

w wall
f fin
i, in inlet
cr critical

References

[1] McEnaney R. P., Park Y. C., Yin J. M., ,Hrnjak P. S.: Performance of the prototype of transcritical R-744 mobile A/C system, SAE International Congress and Exposition, Paper 1999-01-0872, 1999.

[2] Chang Y., J. Wang C. C.: A generalized heat transfer correlation for louver fin geometry, International Journal of Heat and Mass Transfer, vol. 40, n 3, pp. 533-544, 1997.

[3] Chang Y., J. Wang C. C.: Air side performance of brazed aluminium heat exchangers, Journal of Enhanced Heat Transfer, vol. 3, n 1, pp. 15-28, 1996.

[4] Idelchik E., Handbook of Hydraulic Resistance, 3rd Edition, CRC Press, 1994.

[5] Gnielinski V.: New equations for heat and mass transfer in turbulent pipe and channel flow, International Chemical Engineering, vol. 16, pp. 359-368, 1976.

[6] Churchill S. W.: Friction-factor equation spans all fluid flow regimes, Chemical Engineering, vol. 7, pp. 91-92, 1977.

[7] Corberan J. M., De Cordoba P. F., Gonzalvez J., Alias F.: Semiexplicit Method for Wall Temperature Linked Equations (SEWTLE): a General Finite-Volume Technique for the Calculation of complex Heat Exchangers, Numerical Heat Transfer: Part B, vol. 40, pp. 37-59, 2001.

[8] Patankar S. V.: Numerical Heat Transfer and Fluid Flow, Hemisphere, New York, 1980.

[9] Asinari P., Finite-Volume and Finite-Element Hybrid Technique for the Calculation of Complex Heat Exchangers by Semi-Explicit Method for Wall Temperature Linked Equations (SEWTLE), to be published on Numerical Heat Transfer: Part B, 2003.

[10] Kern D. Q., Kraus A. D.: Extended Surface Heat Transfer, McGraw-Hill, New York, 1994.

[11] Yin J. M., Bullard C. W., Hrnjak P. S.: R-744 gas cooler model development and validation, International Journal of Refrigeration, vol. 24, pp. 692-701, 2001.

[12] Rieberer R.: CO2 properties, IIR Workshop on CO2 Technology in Refrigeration, Heat Pump and Air Conditioning Systems, Mainz, Germany, 1999.

[13] Prasad B. S. V.: Fin Efficiency and Mechanisms of Heat Exchange Through Fins in Multi-Streams Plate-Fin Heat Exchangers: Formulation, International Journal of Heat and Mass Transfer, vol. 39, n 2, pp. 419-428, 1996.

Figure Captions

Figure 1. (a) Generic element of compact crossflow heat exchanger. (b) Plan view of control volume centroids. (c) Isometric view of control volume centroids.

Figure 2. (a) Intrinsically conservative element for fin discretisation. (b) Three-dimensional plot of fin temperature field by intrinsically conservative elements.

Figure 3. Basic geometry of the considered heat exchanger. The frontal area is equal to $545 \ x \ 350 \ (h) \ mm$. The number of flat tubes is equal to 34 and they are subdivided into 3 passages [11].

Figure 4. Comparison between total heat flow calculated by numerical code and experimental data [11]. (a) Simulations performed with detailed meshes: Test n° 9, n° 32 and n° 37. (b) Correlation between error and factor E accounting for operation near the critical point.

Figure 5. Contour lines of the splitting factor for conductive heat flow at fin roots (air side frontal view, XZ plane in Fig. 1).

Figure 6. Thermal variables in a fin ($r = 2.47$) located between the first and the second passage. Black arrows refer to conductive heat flows (transverse and longitudinal). Values inside circles refer to convective thermal fluxes. Values inside parentheses refer to half-fin-length idealisation.

Figure 7. Contour lines of parameter σ (temperature variance in the cross sections of flat tubes) (air side frontal view, XZ plane in Fig. 1).

Figure 8. Contours lines of longitudinal conductive heat flow in flat tubes (air side frontal view, XZ plane in Fig. 1).

List of Tables

Table 1

Phenomenological coefficients used in numerical code.

	Heat Transfer	**Pressure Drop**	
		Localized	**Distributed**
	α **[W/m^{2}K]**	f **[-]**	ξ **[-]**
Air	Chang e Wang, 1997 [2]	Chang e Wang, 1996 [3]	Idelchik, 1994 [4]
CO_2	Gnielinski, 1976 [5]	Churchill, 1977 [6]	Idelchik, 1994 [4]

Table 2

Effects of mesh resolution on transferred thermal power.

TEST [11]	Virtual Micro channels	Transferred Thermal Power					
		Measured (1)	Code (2)	I	II	III	Error (2)/(1)
		[W]	[W]	[W]	[W]	[W]	[%]
Test n° 9	1	3643	4041	2418	1027	595	+10.9
Test n° 9	3	3643	3887	2354	976	557	+6.7
Test n° 9	5	3643	3872	2324	975	572	+6.3
Test n° 9	7	3643	3820	2250	975	595	+4.9
Test n° 9	9	3643	3836	2251	978	607	+5.3
Test n° 9	11	3643	3845	2251	987	607	+5.5

Table 3

Effects of pressure drops on transferred thermal power.

TEST [11]	**Pressure Drops**	**Transferred Thermal Power**		
		Measured (1)	**Code (2)**	**Error (2)/(1)**
		[W]	**[W]**	**[%]**
Test n° 9	Δp (Tab. 1)	3643	4041	+10.9
Test n° 9	$2 \cdot \Delta p$	3643	4022	+10.4
Test n° 9	$3 \cdot \Delta p$	3643	4002	+9.9
Test n° 9	$4 \cdot \Delta p$	3643	3983	+9.3

Table 4

Effects of different assumptions in fin modelling on transferred thermal power.

TEST [11]	**Fin Modeling**	**Transferred Thermal Power**		
		Measured (1)	**Code (2)**	**Error (2)/(1)**
		[W]	**[W]**	**[%]**
Test n° 27	Half-Fin-Length Idealization	3285	3420	+4.1
Test n° 27	Improved Temperature Field	3285	3385	+3.0
Test n° 32	Half-Fin-Length Idealization	3596	3918	+9.0
Test n° 32	Improved Temperature Field	3596	3879	+7.9
Test n° 32	Half-Fin-Length Idealization	3138	3353	+6.9
Test n° 32	Improved Temperature Field	3138	3327	+6.0

Table 5

Effects of heat transfer coefficients on transferred thermal power.

TEST [11]	**Heat Transfer Coefficients**	**Transferred Thermal Power**		
		Measured (1)	**Code (2)**	**Variation (2)/(1)**
		[W]	**[W]**	**[%]**
Test n° 11	Reference	4774	4845	+1.5
Test n° 11	α_e +20%	-	4897	+2.6
Test n° 11	α_i +20%	-	4848	+1.6
Test n° 11	λ +20%	-	4843	+1.4
Test n° 32	Reference	3596	3879	+7.9
Test n° 32	α_e +20%	-	4079	+13.4
Test n° 32	α_i +20%	-	3895	+8.3
Test n° 32	λ +20%	-	3882	+8.0

Table 6

Effects of conduction modelling on transferred thermal power.

TEST [11]	Conduction Modeling	Transferred Thermal Power		
		Measured (1) [W]	Code (2) [W]	Variation (2)/(1) [%]
Test n° 11	Reference	4774	4845	+1.5
Test n° 11	No Conduction Longitudinal Fin	-	4844	+1.5
Test n° 11	No Conduction Longitudinal Tube	-	4845	+1.5
Test n° 11	No Conduction Transverse Tube	-	4843	+1.4
Test n° 32	Reference	3596	3879	+7.9
Test n° 32	No Conduction Longitudinal Fin	-	3879	+7.9
Test n° 32	No Conduction Longitudinal Tube	-	3882	+8.0
Test n° 32	No Conduction Transverse Tube	-	3878	+7.8

List of figures

Figure 1

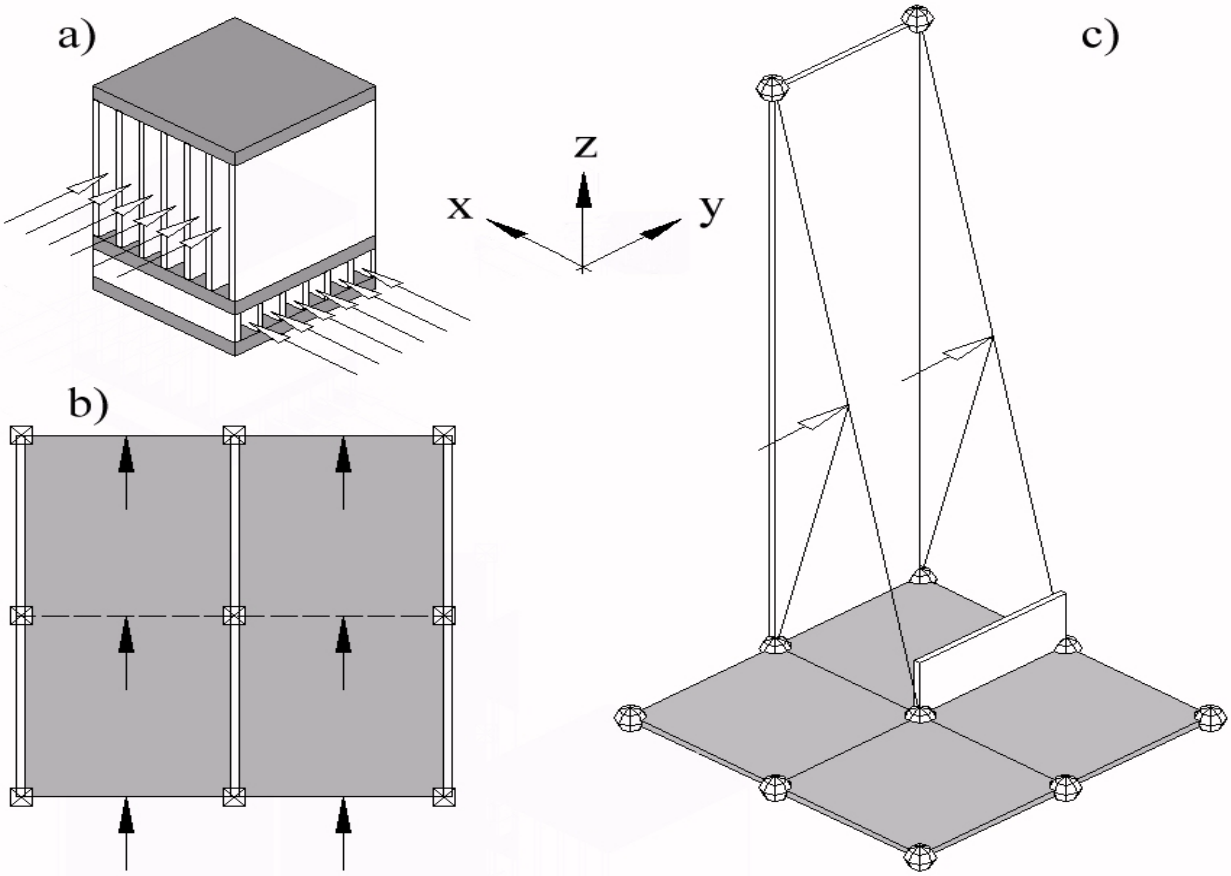

Figure 2

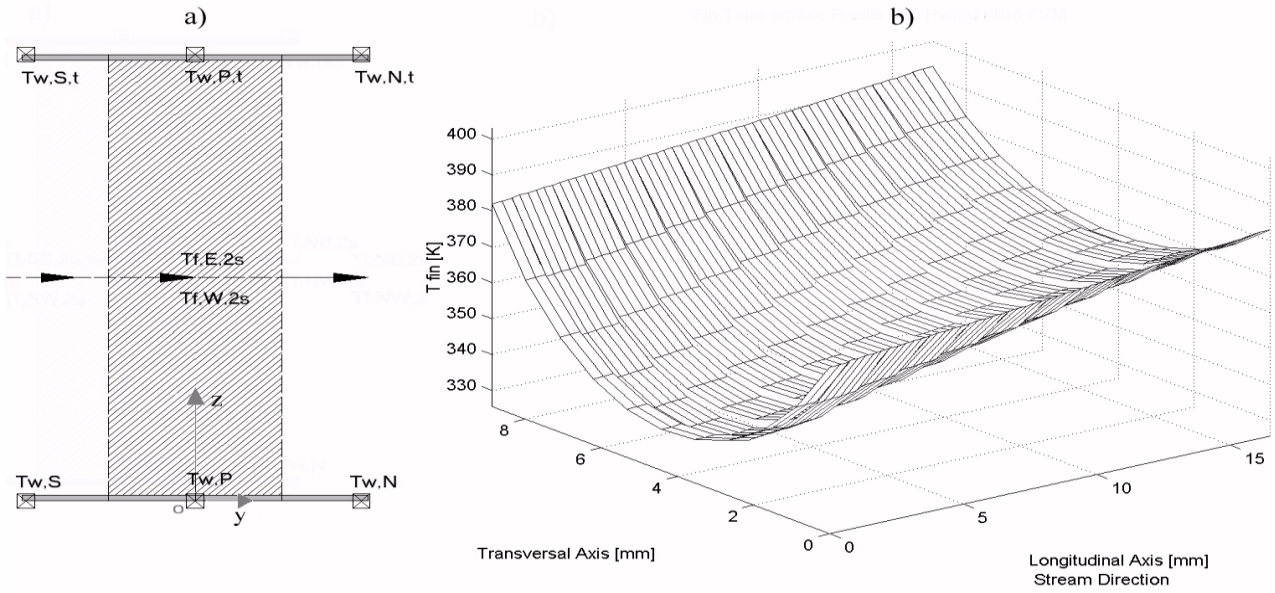
a)
Tw,S,t
Tw,P,t
Tw,N,t
Tf,E,2s
Tf,W,2s
z
Tw,S
Tw,P
Tw,N
o
y
b)
T fin [K]
400
390
380
370
360
350
340
330
8
6
4
2
0
0
5
10
15
Transversal Axis [mm]
Longitudinal Axis [mm]
Stream Direction

Figure 3

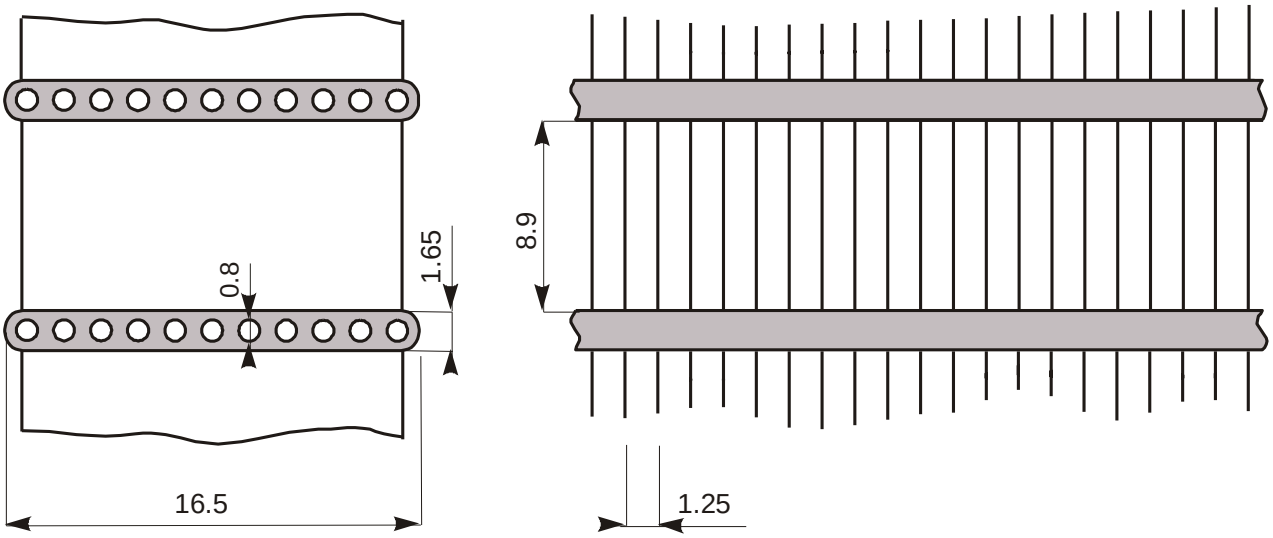

Figure 4

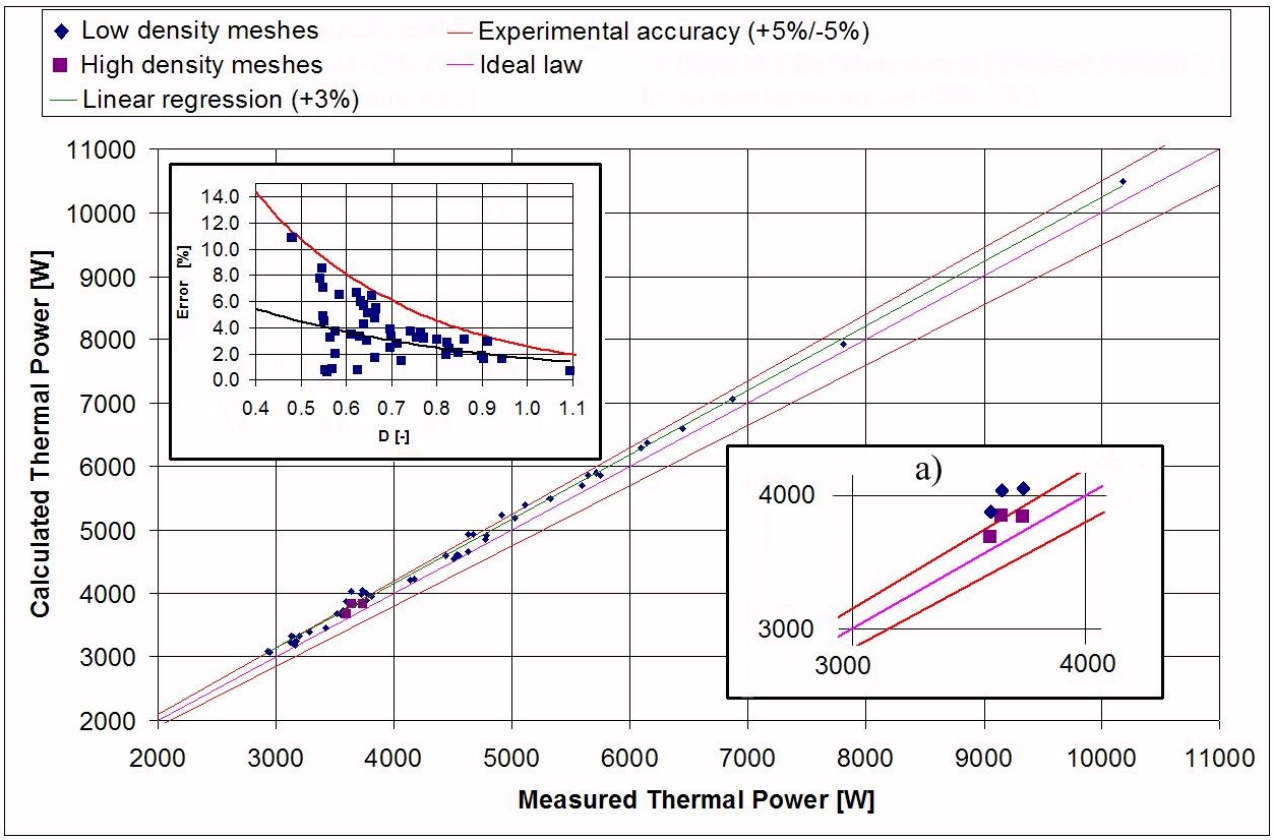
Low density meshes
High density meshes
Linear regression (+3%)
Experimental accuracy (+5%/-5%)
Ideal law
Calculated Thermal Power [W]
Measured Thermal Power [W]
Error [%]
D [-]
a)

Figure 5

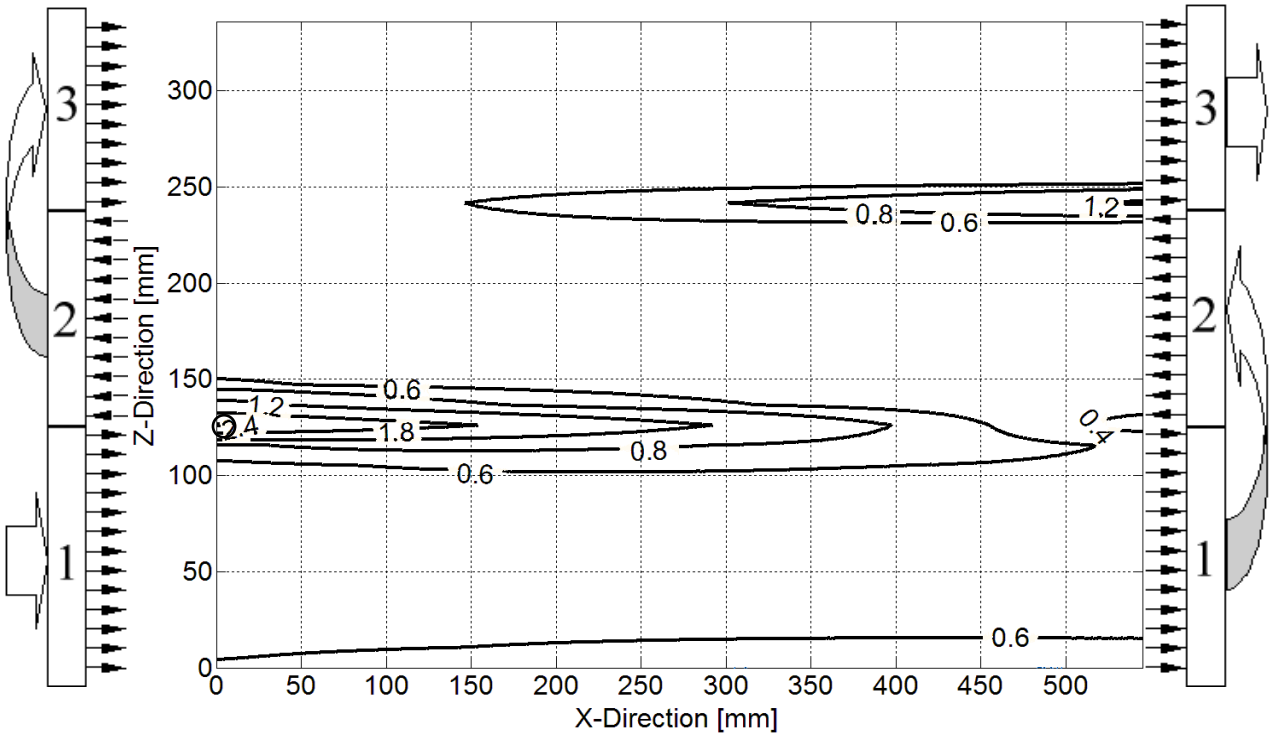
3
2
1
Z-Direction [mm]
X-Direction [mm]
0
50
100
150
200
250
300
350
400
450
500
0.6
1.2
1.8
2.4
0.8
0.6
0.8
1.2
0.4
0.6

Figure 6

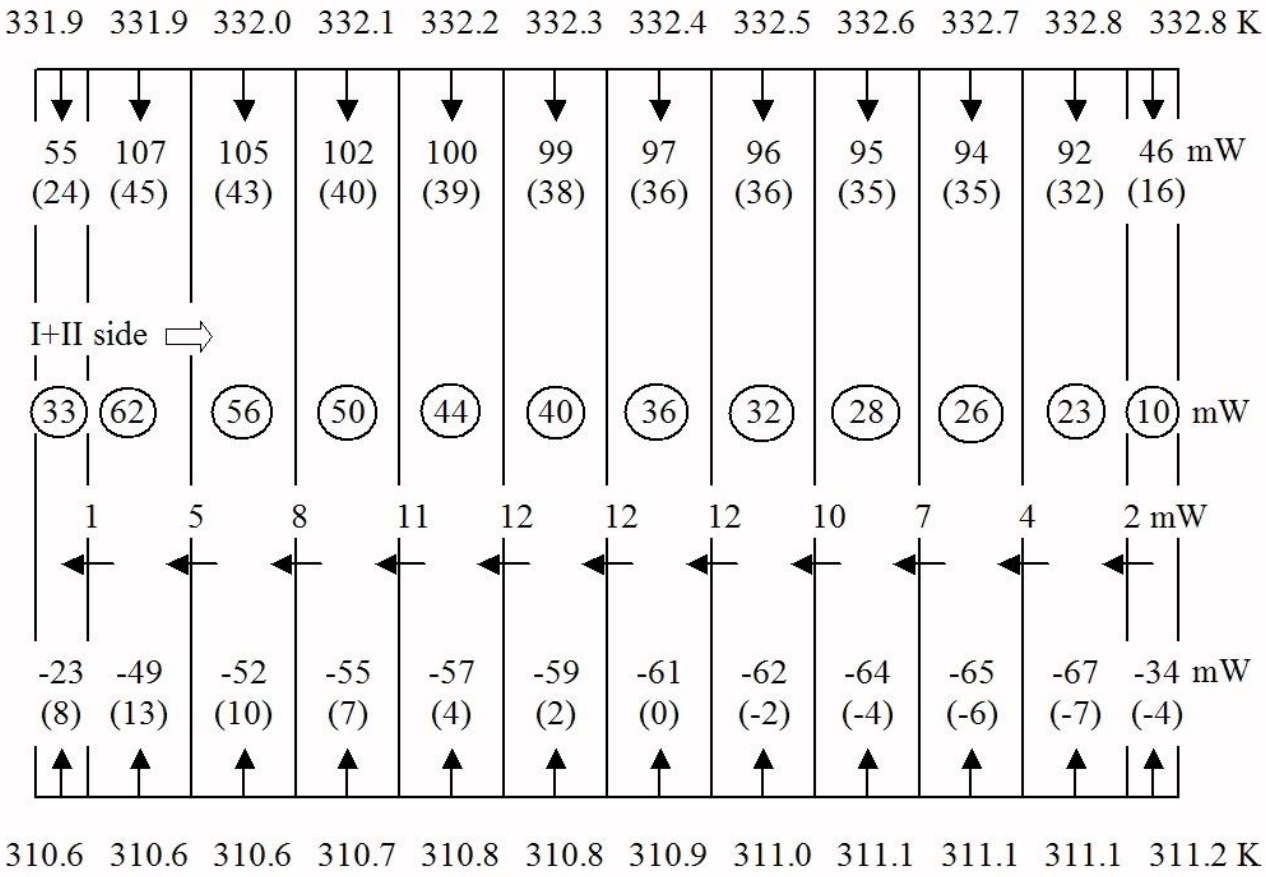
331.9 331.9 332.0 332.1 332.2 332.3 332.4 332.5 332.6 332.7 332.8 332.8 K
55 (24) 107 (45) 105 (43) 102 (40) 100 (39) 99 (38) 97 (36) 96 (36) 95 (35) 94 (35) 92 (32) 46 (16) mW
I+II side
33 62 56 50 44 40 36 32 28 26 23 10 mW
1 5 8 11 12 12 12 10 7 4 2 mW
-23 (8) -49 (13) -52 (10) -55 (7) -57 (4) -59 (2) -61 (0) -62 (-2) -64 (-4) -65 (-6) -67 (-7) -34 (-4) mW
310.6 310.6 310.6 310.7 310.8 310.8 310.9 311.0 311.1 311.1 311.1 311.2 K

Figure 7

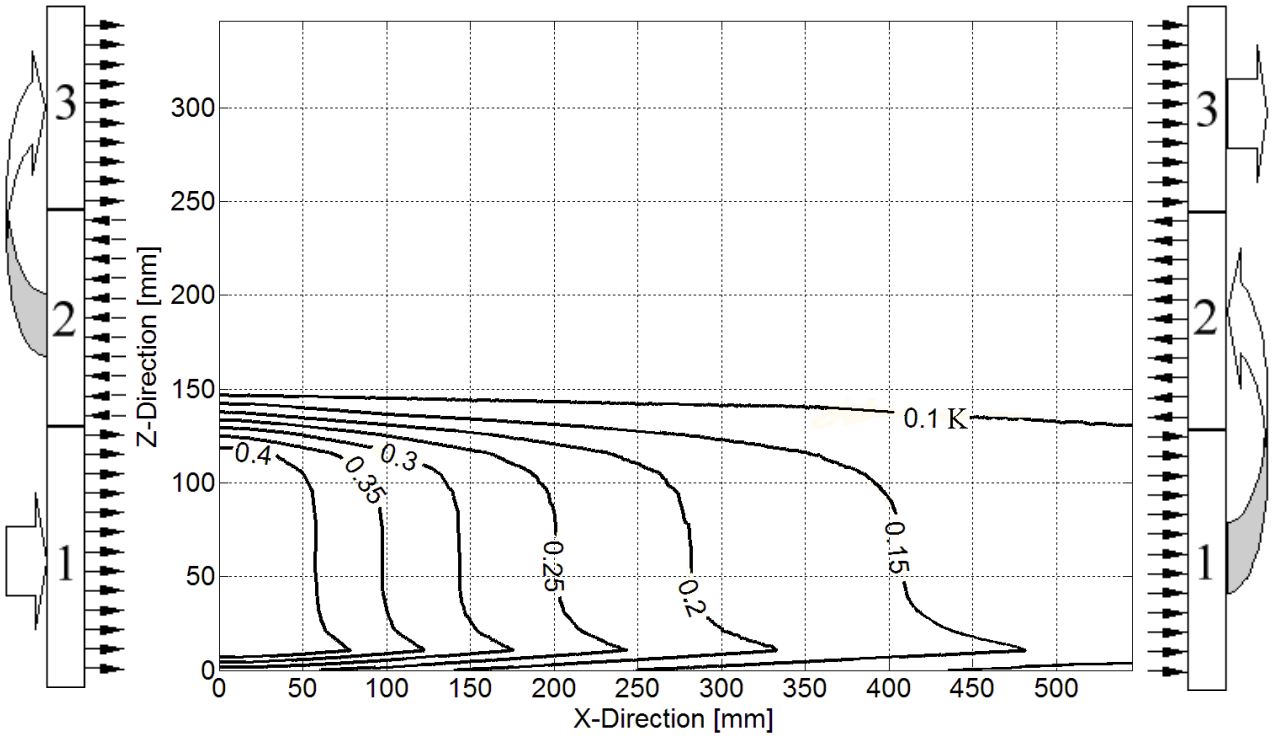
3
2
1
Z-Direction [mm]
300
250
200
150
100
50
0
0.1 K
0.4
0.35
0.3
0.25
0.2
0.15
0
50
100
150
200
250
300
350
400
450
500
X-Direction [mm]
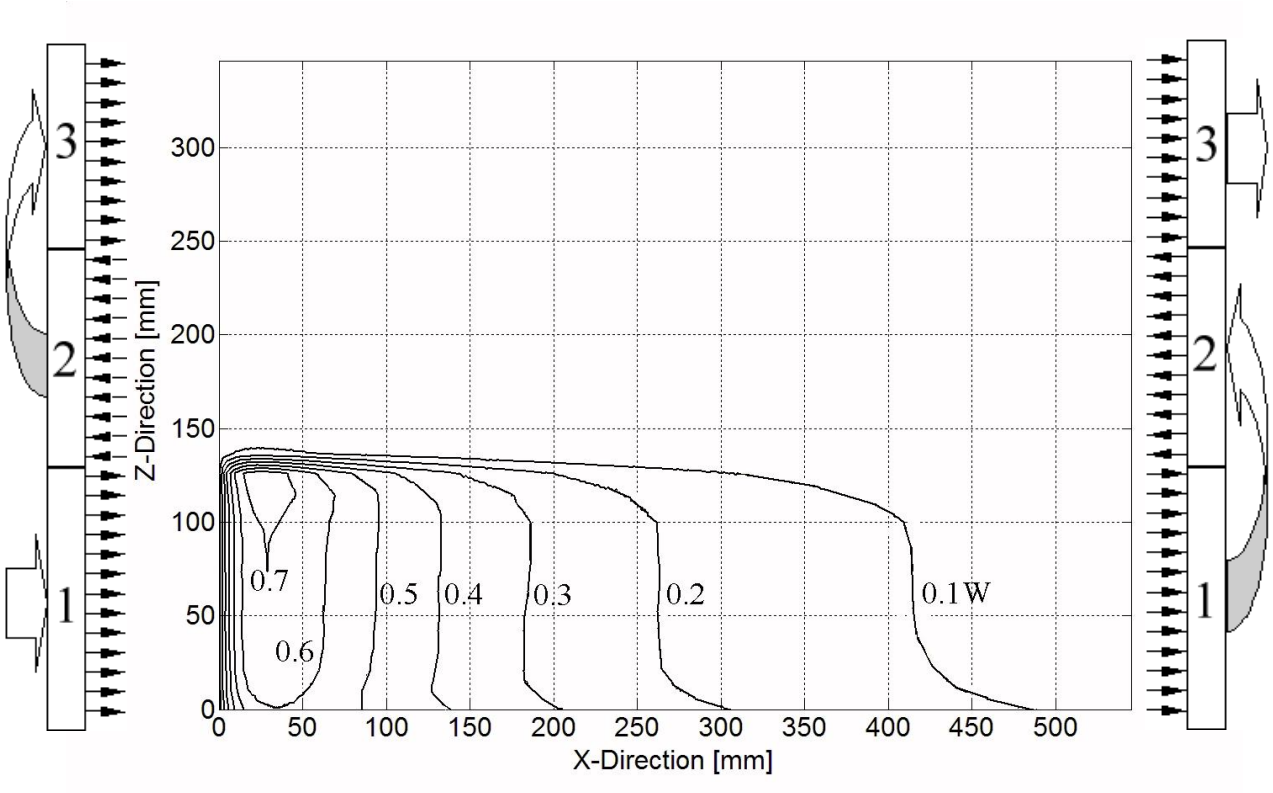
Figure 8